Increasing P-wave and S-wave velocity resolution with FWI — a North Sea shallow water case study

Alireza Roodaki[1]*, Loic Janot[1], Manuel Peiro[1], Hao Jiang[1], Wenlei Gao[1], Hervé Prigent[1], Ziqin Yu[1], Nabil Masmoudi[1], Andrew Ratcliffe[1], Per Eivind Dhelie[2], Vidar Danielsen[2], Knut Richard Straith[2] and Arnstein Kvilhaug[2].

Abstract

Multi-component data recorded during Ocean-Bottom Seismic (OBS) surveys captures both PP and PS events. PP and PS images provide complementary information about reservoir properties. The quality of both these types of images depends on the accuracy of the P-wave and S-wave velocity models, V_P and V_S, respectively. In this paper, focusing on data from a shallow water OBS survey in the Central North Sea, we show, first, how a high-resolution 65 Hz V_P model, obtained using Time-Lag FWI, can improve the imaging from the shallow to the deep. Similar improvements are then shown for PS data using a 30 Hz V_S model obtained from PS reflection-FWI. The most remarkable achievement is the flattening of the undulating chalk and top reservoir surfaces on both the V_P and V_S FWI Images, obtained from PP and PS data, respectively, which was confirmed by drilling observations. These derived V_P and V_S FWI Images reduce the uncertainty in reservoir characterisation.

Introduction

Ocean Bottom Cable (OBC) surveys attract considerable industry interest for reservoir imaging as they record wide-azimuth broadband data with long offsets. They also ensure high repeatability which is an important parameter for reservoir monitoring. With four components recording PP and PS waves, they can bring more insight to reservoir characterisation and lithology analysis (Colnard et al., 2019). The quality of PP and PS images depends highly on the accuracy of the P-wave, V_P, and S-wave, V_S, velocity models.

Recent developments in Full-Waveform Inversion (FWI), such as Time-Lag FWI (TLFWI, Zhang et al., 2018), together with higher computational capabilities, allow us to produce high-resolution V_P FWI models with frequencies exceeding 50 Hz (Salaun et al., 2021). By capturing lateral and vertical velocity variations, these high-resolution FWI velocity models improve the imaging of structures from shallow to deep. It is also possible to obtain a direct estimate of the PP reflectivity through FWI Imaging (Zhang et al., 2020).

Owing to difficulties in building a V_S model honouring high-resolution vertical and lateral velocity variations in the overburden, the PS image is often of low quality compared to the PP image. Conventional V_S model building from PS reflection data relies on PS (or joint PP-PS) tomography and event registration. This method has many limitations, particularly the fact that the updated V_S model lacks high-resolution information. Full-wavefield-based methods make it possible to achieve higher resolution. Elastic FWI would be the most accurate approach for retrieving a V_S model, but it remains difficult owing to the computational cost of elastic full-waveform modeling at high frequency. As an alternative, quasi-elastic Born modeling can be used (Feng and Schuster, 2019). In this approach, the PS-reflected wavefield is approximated by a formula using acoustic wavefields propagating in the V_P and V_S background models. Based on an approximation of this quasi-elastic Born modelling, Masmoudi et al. (2021) proposed an adaptation of Reflection-FWI (RFWI; Xu et al., 2012) to PS data, which can be used to update the background V_S model (V_{0S}). Later, Peiro et al. (2022) proposed an extension of the method to obtain a high-wavenumber perturbation model, δV_S.

Here, on a shallow water OBC data set over the Edvard Grieg field in the Central North Sea, we present results from an FWI V_P update up to 65 Hz using P and Z components, and the results of PS-RFWI run to update the V_S velocity model up to 30 Hz using a preprocessed radial component.

Edvard Grieg field OBC data

Edvard Grieg is an oil field in the Central North Sea, located approximately 180 km west of Stavanger on the Utsira High platform. The reservoir interval is less than 50 m thick, beneath a high-impedance chalk layer at a depth of approximately 2 km. Building an accurate velocity model for this field presents many challenges:

[1] CGG | [2] Aker BP

* Corresponding author, E-mail: alireza.roodaki@cgg.com

DOI: 10.3997/1365-2397.fb2024037

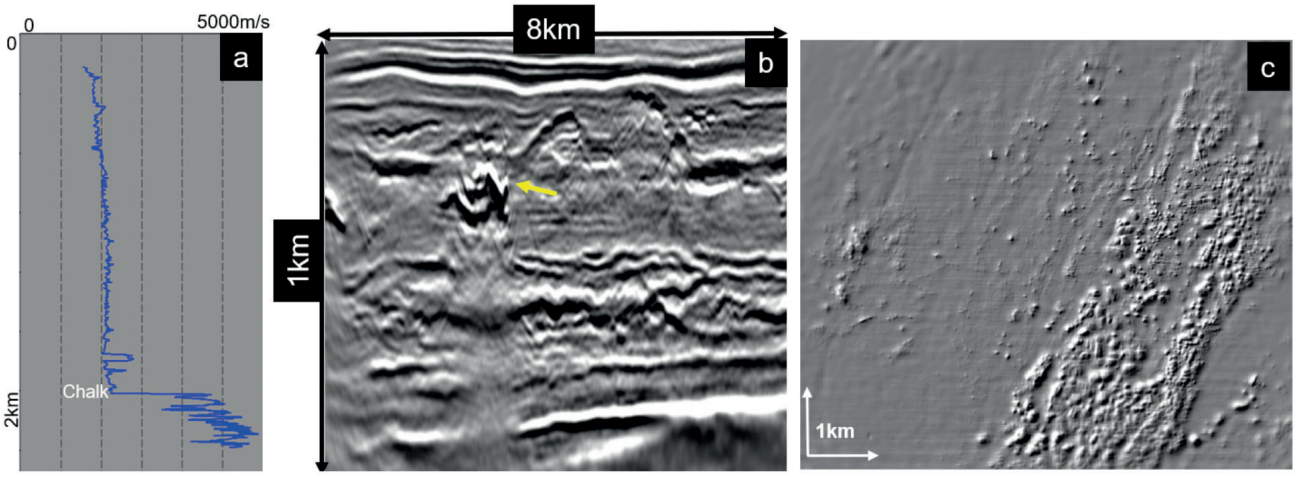

Figure 1 (a) V_p sonic log, (b) RTM section featuring an injectite body, (c) depth slice at 360 m showing gas pockets.

- There are not many vertical velocity variations down to the chalk (Figure 1-a). Long offsets (more than 10 km) are therefore required to record the diving waves needed for FWI to update the velocity down to the reservoir level. Fortunately, the OBC data presented here were acquired with offsets of up to 13 km.
- The presence of high-contrast geological features called injectites (yellow arrow in Figure 1-b). These are compressed sand bodies and their velocity can be 1000 m/s higher than the velocity of the surrounding rocks. They cause issues not only for velocity model-building but also for imaging, as a loss of illumination is generally observed below these features.
- Lateral velocity variations in the shallow part of the section due to the presence of gas pockets and channels (Figure 1-c). These features have a relatively low velocity compared to the neighbouring background velocity and need to be taken into account in the velocity model to avoid imaging problems in the deeper section.

Strong lateral velocity variations make imaging and reservoir characterisation challenging. In fact, not taking into account the shallow lateral velocity variations and the injectites resulted in deep structural undulations on legacy images. This led to confusion when comparing the PP reflectivity (Kirchhoff PSDM) with measurements from drilled horizontal wells. One example is shown in Figure 2, where the legacy image (top) led to the interpretation of a graben structure with fault displacement whereas when the distance from the wellbore to the top reservoir seal was measured using a deep resistivity logging tool during drilling (bottom) it became clear that this graben was absent and that the reservoir structure was simpler (Dhelie et al., 2022).

These seismic depth undulations are very troublesome when it comes to the placement of future production wells as they affect definition of the reservoir structure. This has been an ongoing issue for a while, and no solution using seismic data was found until recently.

Regular OBC campaigns were acquired over this field (Twynam et al., 2020) for 4D monitoring purposes. In this article, we present results obtained from data acquired in 2018, with 44 receiver cables laid out on the sea floor with a receiver grid of 25 m x 200 m and a dense shot carpet of 25 m x 50 m with a maximum offset of 13 km.

High-resolution reservoir compartment delineation using FWI

FWI derives high-resolution velocity models by minimising the difference between observed and modelled seismic waveforms. It goes beyond refraction and reflection tomography techniques by using additional information provided by the full seismic wavefield, including diving waves, reflections and their ghosts and multiples. From this detailed velocity field, it is then possible to derive the reflectivity, called the FWI Image (Zhang et al., 2020).

Figures 3-a and 3-c, respectively, show the legacy V_P velocity model, used as an initial model for FWI, and its corresponding Kirchhoff PSDM cube on two sections. We can observe on the seismic images that the chalk structure suffers from undulations

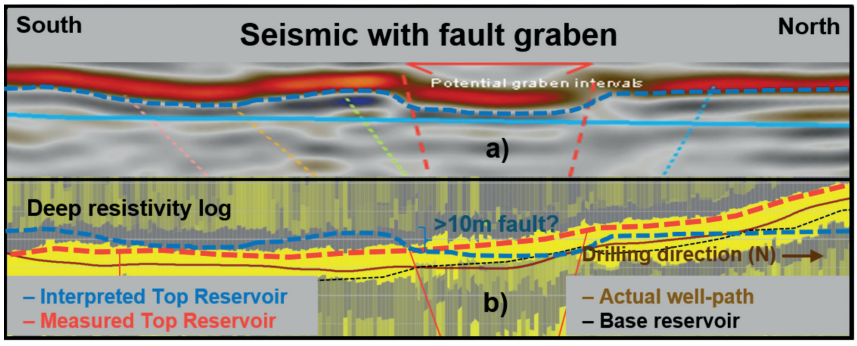

Figure 2 a) original seismic section indicating a graben structure with a possible fault displacement of more than 10 m. b) during drilling it became clear that this graben was not present and the Top Reservoir (red dotted line) was almost flat.

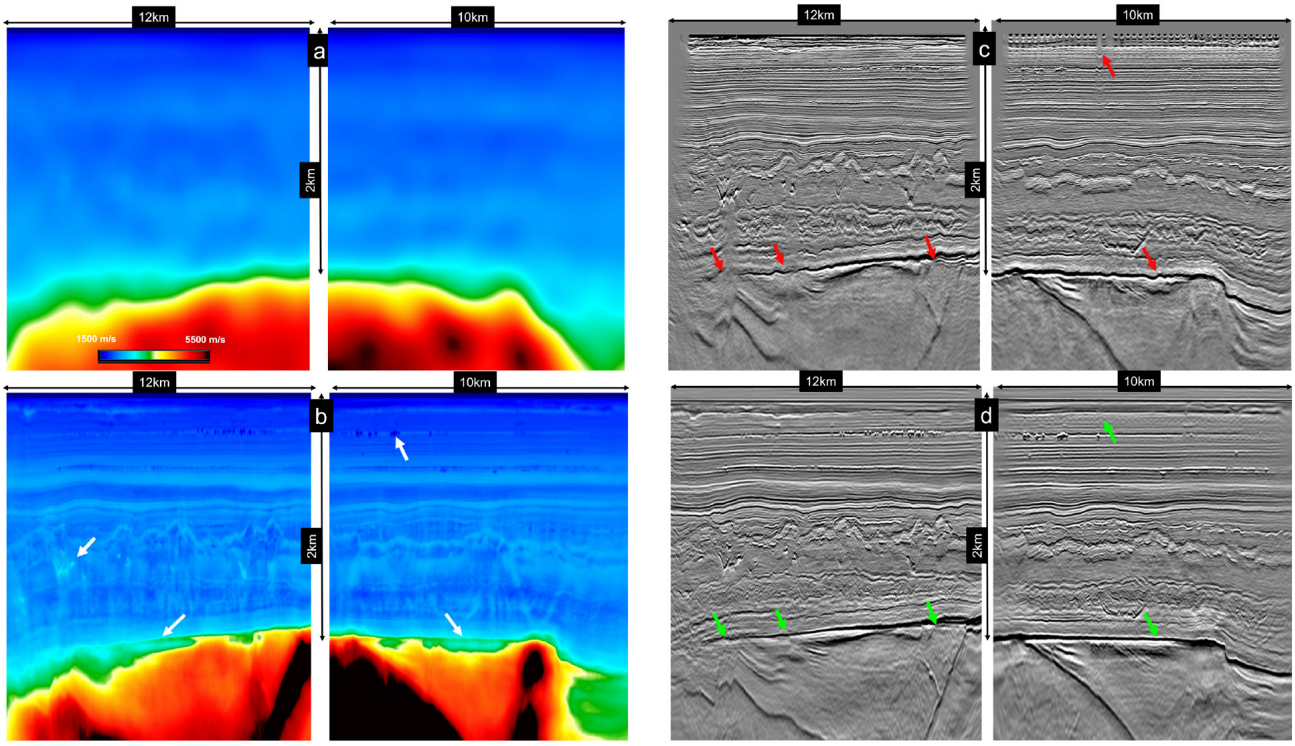

Figure 3 Legacy V_p velocity (a) and its corresponding Kirchhoff PSDM image filtered at 65 Hz (c). 65 Hz FWI V_p velocity with white arrows indicating small features captured by the high-resolution FWI velocity update (b) and its corresponding FWI Image (d). Red and green arrows in figures (c) and (d) indicate areas where high-resolution FWI improved the imaging compared to the legacy image.

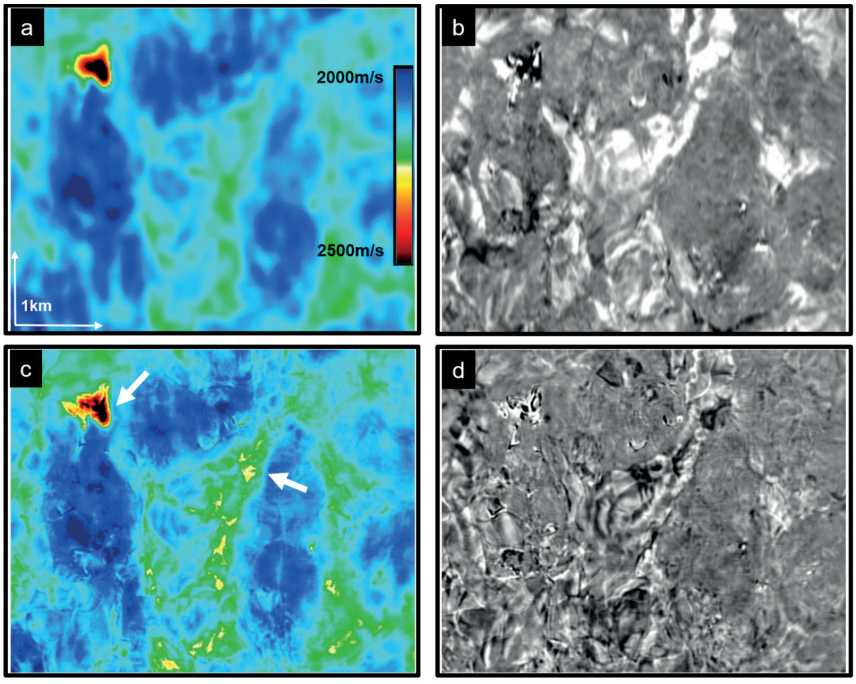

Figure 4 20 Hz FWI V_p velocity (a) and its corresponding Kirchhoff PSDM filtered at 65 Hz image depth slice (b). 65 Hz FWI V_p velocity (c) and its corresponding FWI Image depth slice. White arrows show examples of where resolution is gained.

and discontinuity below the injectites. We ran FWI from PP data recorded by the hydrophone and the vertical geophone sensors. Figure 3-b shows the high-resolution V_P velocity model obtained up to 65 Hz. We can see that many geological features have been captured in this very detailed model, from low-velocity gas pockets in the shallow part to high-velocity injectites in the middle of the section and the high-contrast chalk reflector in the deeper part indicated by the white arrows. The resulting FWI Image (Figure 3-d) exhibits a much-simplified reservoir structure and improved continuity of the chalk, particularly below the injectites. Note that, since FWI uses the full wavefield (with ghosts and multiples), it extends the imaging coverage and enhances imaging in the shallow section, noticeably filling the platform hole.

Figure 4 compares the FWI V_P velocity models at 20 Hz (a) and at 65 Hz (c). It also compares the Kirchhoff PSDM filtered at 65 Hz (b) and FWI Images (d) using these two velocity models.

It illustrates the enhanced imaging of injectites and faults when inverting for a higher-frequency velocity model. We can observe that these high-resolution events are also easily detectable on the 65 Hz model.

Figures 5-c and 5-d compare Kirchhoff PSDM sections filtered at 65 Hz using the legacy velocity and the FWI model. We observe that using an accurate velocity model can significantly improve the imaging of structures and reduce the wobbling. The well trajectory (black line) coincides with the reservoir beneath the chalk, whereas it does not match in the legacy image. Moreover, the interpreted chalk horizon is smoother when using the FWI model (Figure 5-b) than when it was interpreted on the legacy image (Figure 5-a). Figure 5-e compares a well sonic profile to the legacy and FWI V_P velocity models. Starting from a smooth initial velocity, FWI managed to capture fine vertical velocity variations and the obtained V_P provides a good match to the sonic profile.

To better appreciate the high-resolution information brought to the velocity model by FWI up to 65 Hz at the reservoir level, Figure 6 (left) presents an overview of the field. Four different expected facies are displayed with their respective colours in the legend. The production and injection wells are drawn respectively in blue and green. Depth sections of the legacy and the 65 Hz FWI V_P velocity models are shown in the middle and right panels of Figure 6. We observe that FWI honours the main geological trends in the reservoir and that the velocity contrasts on the section correlate well with variations in reservoir facies.

Reconciling V_S and V_P FWI Images using PS-RFWI

Having obtained a high-resolution V_P velocity model that resolved many imaging issues, the next challenge was to generate a high-resolution V_S velocity model with similar properties. The methodology used to estimate the S-wave velocity is based on a Born approximation-based PS-RFWI (Masmoudi et al., 2021; Peiro et al., 2022). As with other FWI methods, PS-RFWI minimises the difference between the observed and modelled PS data through optimisation of an objective function J. The FWI gradients for the background V_{0S} and the perturbation δV_S models can be obtained via the adjoint-state method, as follows:

$$\frac{\partial J}{\partial V_{0S}} = \int_{t=0}^{tmax} \frac{\partial \delta S(t)}{\partial V_{0S}} R(t)\, dt, \quad (1)$$

$$\frac{\partial J}{\partial \delta V_S} = \int_{t=0}^{tmax} -\frac{\partial^2 P(t)}{\partial t^2} R(t)\, dt, \quad (2)$$

where δS is the scattered S-wavefield propagating in the background V_{0S} model, P is the incident P-wavefield propagating in the background V_{0P} model, and R is the adjoint S-wavefield obtained by backpropagating the residuals of the PS-reflection data injected at the receiver positions.

The input seismic data to PS-RFWI was the preprocessed radial component of the receiver gathers, that were multiple- and ghost-free. Like all inversion methods, PS-RFWI is sensitive to the initial model. To build the initial V_S model, we used a smoothed and edited version of the FWI V_P model, scaled by a V_P/V_S ratio derived from P- and S-sonic logs. To refine the very shallow part of the V_S initial model (down to 200 m), a multi-wave inversion step (Bardainne, 2018) was run using the surface waves recorded on the Z component. Finally, a PP-PS registration was performed to match the PP and PS interpreted horizons and to register the V_S model with respect to the V_P one.

The V_S model was then updated in two steps: first, the background V_{0S} model and, second, the high-resolution perturbation δV_S model. The perturbation δV_S update was then combined with the background V_{0S} model to obtain the final V_S model that should correct for kinematics and depthing of events while featuring high-resolution details.

Figure 7 compares the legacy V_S model (a) and the final (b), fully updated, 30 Hz V_S model, coming from the combined background and perturbation models, as well as their corresponding image sections. The final V_S model, Figure 7-c, highlights rich vertical and lateral details consistent with the main geological events visible on the seismic sections and shows good agreement with the well-log data in Figure 7-e. The V_S FWI Image is derived from the final V_S model and is shown in Figure 7-d. This demonstrates a geologically consistent section, relative to the V_P FWI Image, from the overburden to the deep, and can be compared with the 30 Hz converted-wave reverse time migration (PS-RTM) from the legacy

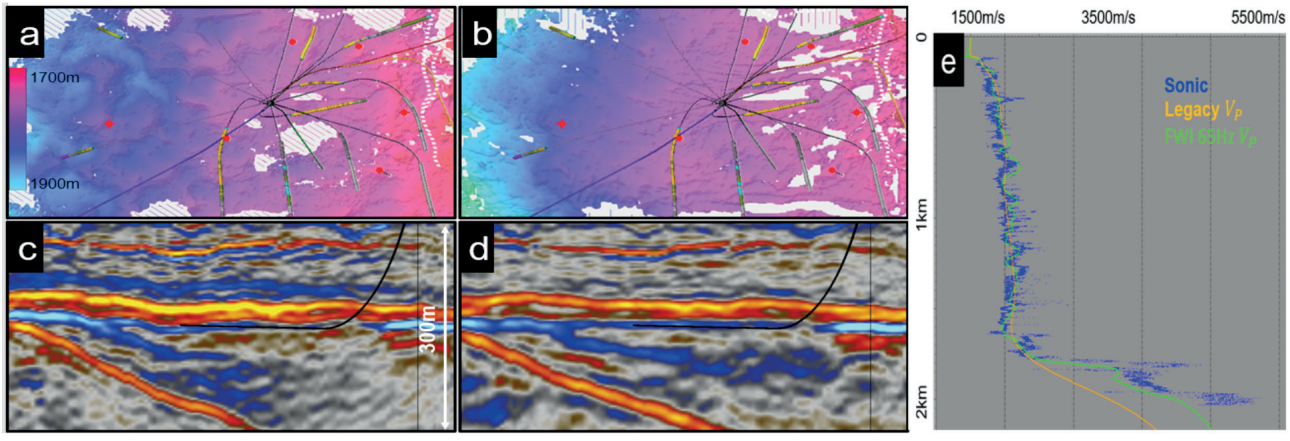

Figure 5 Interpreted chalk horizon on a Kirchhoff PSDM image using the legacy velocity model (a) and FWI model (b). Corresponding Kirchhoff images for the legacy (c) and FWI model (d), with the well trajectory indicated by the black line. (e) Comparison of legacy (orange line) and FWI velocity models (green line) with the well sonic profile (blue line).

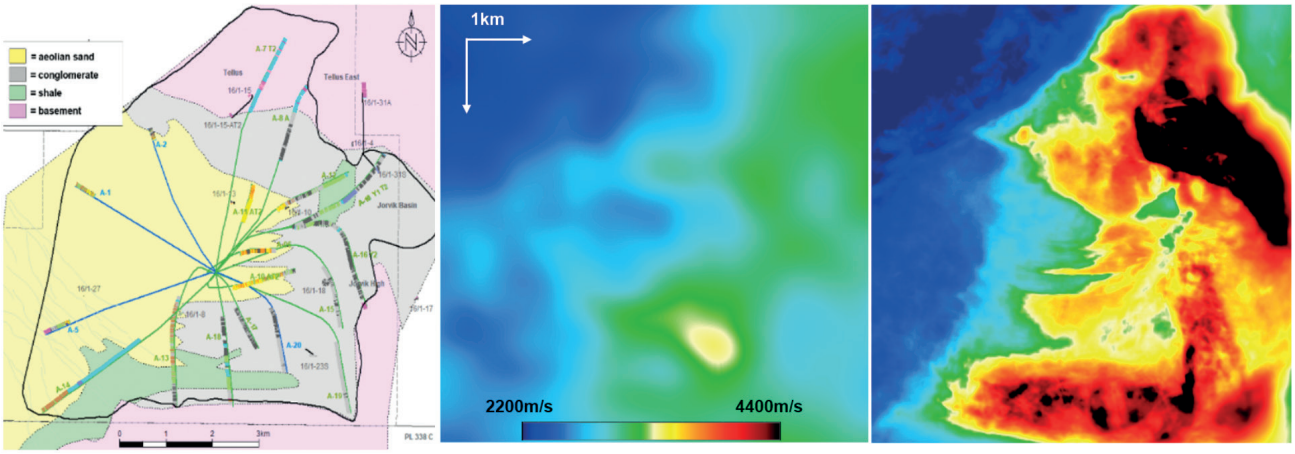

Figure 6 Edvard Grieg reservoir facies (left), depth slice at 1900 m for the legacy V_p velocity (middle) and for 65 Hz FWI V_p velocity (right).

model (Figure 7-b). Overall, in the new V_S FWI Image the chalk appears flatter, the signal-to-noise ratio is improved at reservoir level and the Base Cretaceous Unconformity (BCU), indicated by arrows, is better imaged thanks to the least-squares process embedded in the PS-RFWI algorithm.

A comparison of the V_S FWI Image with the legacy 30 Hz PS-RTM section (Figure 8) reveals that the new PS-based workflow led to similar improvements to those observed in the V_P FWI Image (Figure 3) and shows good consistency with the V_P FWI Image, also shown in Figure 8. Furthermore, we can see that the V_S FWI image has comparable resolution to the V_P FWI image above the chalk horizon (green line on Figure 8). We also observe imaging differences in some of the geological features. For example, the clean sands above the reservoir zone are brighter on the V_S FWI Image, as expected from well data. However, the V_P FWI image has a finer resolution beneath the chalk. We believe this is because of the higher signal-to-noise-ratio of the PP-data relative to the PS-data in this deep region. This is evidenced by looking at either of the PS-RTM images (Figure 7-b or the middle panel of Figure 8), where we observe an absence of higher frequencies in the PS recorded data below the chalk, relative to the data quality above the chalk.

At this stage it is worth highlighting that the V_P FWI image shown in Figure 8 was obtained at 65 Hz and subsequently filtered back to 30 Hz. Moreover, the V_P FWI image uses all parts of the wavefield, i.e., primaries, multiples, and diving-waves. Therefore, in general, we would expect it to have better imaging properties compared to PS-RFWI that only uses primaries. Other known limitations of PS-RFWI are the need to correctly isolate the PS-reflections, the single-scattering assumption of Born modelling, and reliance on acoustically modelled PS data, with its known potential amplitude discrepancies between modelled and observed data. In our case, the impact of these issues could be handled with an appropriate FWI cost function and reliable well

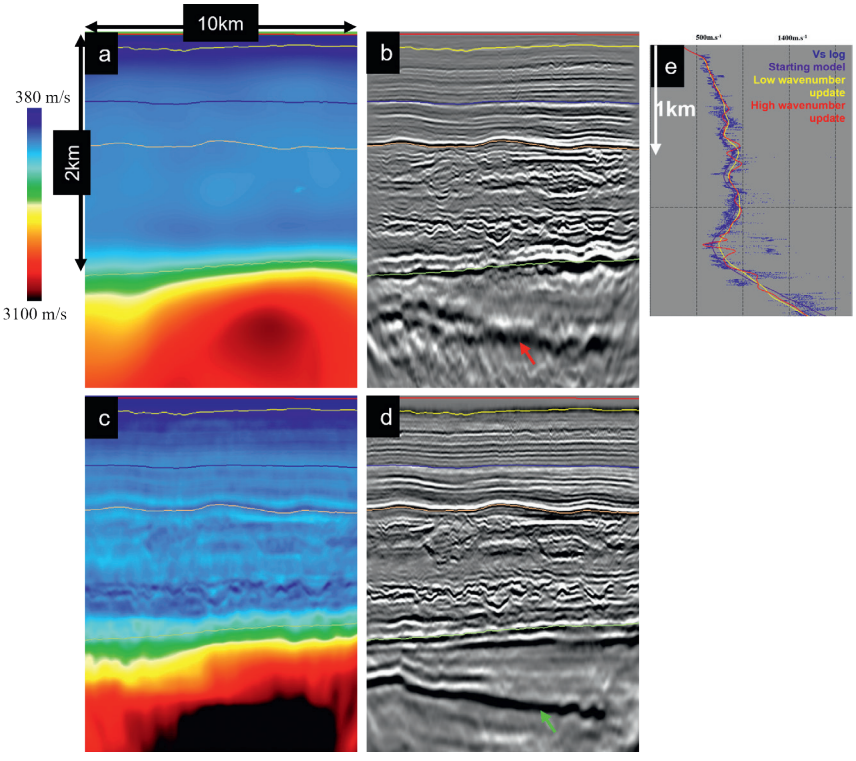

Figure 7 Legacy V_S model (a) and its corresponding 30 Hz PS-RTM migrated section (b). 30 Hz V_S model (c) and its corresponding V_S FWI Image (d). The green line on the seismic sections indicates the PP chalk horizon while arrows (red and green) indicate BCU. (e) Comparison of starting model (purple line), low wavenumber V_S (yellow line) and high wavenumber V_S (red line) with the well V_S sonic profile (blue line).

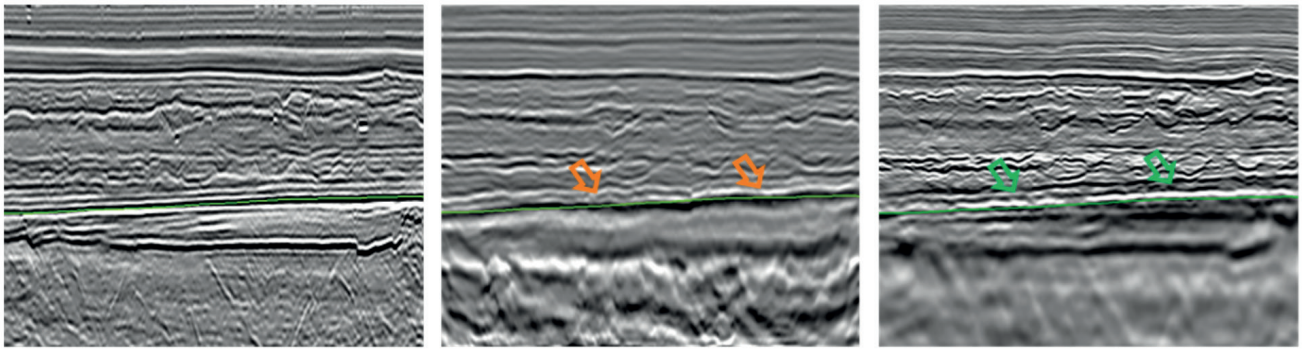

Figure 8 Comparison of the V_P FWI Image filtered to 30 Hz (left), the legacy 30 Hz PS-RTM image (middle), and the 30 Hz V_S FWI Image (right). The latter improves the flatness of the chalk (green line and arrows) and the reservoir below that matches with the image from the PP data.

information. Finally, the crosstalk between V_P and V_S might not be fully addressed due to acoustic approximation, although our workflow endeavours to mitigate this by using the PP reflectivity obtained from the V_P FWI.

Conclusion

The Edvard Grieg field turns out to be an exciting playground for new FWI developments. We have presented here how a sequential use of TLFWI – from the two vertical OBC components – and PS-RFWI – from the two horizontal components – can generate high-resolution V_P and V_S velocity models and resolve imaging issues. The most remarkable achievement is the flattening of the undulating chalk and top reservoir surfaces on both the V_P and V_S FWI Images, obtained from PP and PS data, respectively, which was confirmed by drilling observations. These derived V_P and V_S FWI Images reduce the uncertainty in reservoir characterisation.

As discussed above, PS-RFWI presents a few known limitations, leaving the door open to multi-component elastic FWI in the not-too-distant future. Nonetheless, the workflow presented here paves the way for obtaining high-resolution V_S FWI models. More accurate V_S models can reinforce the use of PS imaging for reservoir characterisation and field monitoring.

Acknowledgements

We would like to thank Aker BP and their partners in PL338, Wintershall Dea and OMV, and CGG for permission to publish this work. We also thank Nicolas Salaun, Daniela Donno, Adel Khalil and Zhigang Zhang for valuable discussions.

References

Bardainne, T. [2018]. Joint inversion of refracted P-waves, surface waves and reflectivity. *80th EAGE Conference & Exhibition, Extended Abstracts, We K 02.*

Colnard, O., Loh, F.C., Doshi, R., Barkov, A., Lyandres, A., Lam Anh, N., Van Thanh, P., Van Khuong, V., Tien Vien, P., Gataulin, R., Geideko, O., Litunovsky, A. and Trong Khanh, N. [2019]. PP/PS Processing, Inversion and Interpretation of Vietnam's First 3D-4C OBC Survey in the Cuu Long Basin. *81st EAGE Conference & Exhibition, Extended Abstracts.*

Dhelie, P.E., Danielsen, V., Haugen, J.A., Straith, K.R., Bakke, B.A., Janot, L, Roodaki, A. and Yu, Z. [2022]. Improved Reservoir Image and Well Placement Using Time-Lag Full Waveform Inversion. *83rd EAGE Conference & Exhibition, Extended Abstracts.*

Feng, Z. and Schuster, G. [2019]. True-amplitude linearized waveform inversion with the quasi-elastic wave equation. *Geophysics*, **84**(6), 827-844.

Masmoudi, N., Ratcliffe, A., Wang, M., Xie, Y. and Wang, T. [2021]. A practical implementation of converted-wave reflection full-waveform inversion. *82nd EAGE Conference & Exhibition, Extended Abstracts.*

Peiro, M., Gao, W., Fotsoh, A., Masmoudi, N., Roodaki, A., Ratcliffe, A., Prigent, H., Leblanc, O. & Dhelie, P.E., Danielsen, V., Haugen, J.A. and Straith, K.R. [2022]. PS Imaging on the Edvard Grieg Field: Application of PS Reflection FWI and FWI Imaging. *83rd EAGE Conference & Exhibition, Extended Abstracts.*

Salaun, N., Reinier, M., Espin, I. and Gigou, G. [2021]. FWI velocity and imaging: A case study in the Johan Castberg area. *82nd EAGE Conference & Exhibition, Extended Abstracts.*

Twynam, F., Ford, R., Caprioli, P., Hooke, M., Whitebread, R., Dhelie, P.E., Danielsen, V. and Straith, K.R. [2020]. Improved reservoir monitoring with PP & PS time-lapse imaging utilising up/down deconvolution: Edvard Grieg field. *81st EAGE Conference & Exhibition, Extended Abstract.*

Xu, S., Chen, F., Lambaré, G., Zhang, Y. and Wang. D. [2012]. Inversion on reflected seismic wave. *82nd Annual International Meeting, SEG, Expanded Abstracts.*

Zhang, Z., Mei, J., Lin, F., Huang, R. and Wang, P. [2018]. Correcting for salt misinterpretation with full waveform inversion. *88th Annual International Meeting, SEG, Expanded Abstracts,* 143-1147.

Zhang, Z., Wu, Z., Wei, Z., Mei, J., Huang, R. and Wang, P. [2020]. FWI Imaging: Full-wavefield imaging through full-waveform inversion. 90th Annual International Meeting, *SEG, Expanded Abstracts*, 656-660.